Microporous and Mesoporous Materials 323 (2021) 111183

Contents lists available at ScienceDirect

Microporous and Mesoporous Materials

journal homepage: www.elsevier.com/locate/micromeso

Supramolecular assembly of L-Lysine on ZSM-5 zeolites with different Si/Al ratio

Tatiana Chenet [a], Annalisa Martucci [b,**], Mirco Cescon [a], Giulia Vergine [a], Giada Beltrami [b], Lara Gigli [c], Matteo Ardit [b], Massimo Migliori [d], Enrico Catizzone [d,1], Girolamo Giordano [d], Luisa Pasti [a,*]

[a] Department of Chemical, Pharmaceutical and Agricultural Sciences, University of Ferrara, Via L. Borsari, 46, 44121, Ferrara, Italy
[b] Physics and Earth Sciences Department, University of Ferrara, Via Saragat 1, 44122, Ferrara, Italy
[c] Elettra - Sincrotrone Trieste, ss 14, km 163.5, Basovizza, 34149, Trieste, Italy
[d] Laboratory of Catalysis and Industrial Chemistry, University of Calabria, Via P. Bucci, Rende, I-87036, Italy

ARTICLE INFO

Keywords:
Amino acids
Zeolite
Self-assembly process
Adsorption

ABSTRACT

The adsorption of the amino acid, L-lysine, on two ZSM-5 having different silicon to aluminium ratio (i.e. Si/Al = 15 and 37) has been investigated by experiments at macroscopic and at atomistic level resolution. The kinetic and equilibrium constants of the adsorption processes obtained for both the adsorption materials, show that Al content is an important factor in tuning the adsorption of the amino acid on the zeolite. Both the saturation capacity and the binding constant decrease as Si/Al ratio increases. The refinements of high resolution X-ray diffraction data obtained from synchrotron radiation, indicate that adsorption of L-lysine in ZSM-5 is a surface-confined supramolecular self-assembly process. L-lysine molecules at the intersection of the sinusoidal and the straight channels, are arranged in a α-helical conformation stabilized by the simultaneous occurrence of strong H-bonds among the tail of L-lysine molecules, water molecules and framework oxygens. L-lysine molecules within the sinusoidal channel are arranged as β-sheets forming infinite hydrogen-bonding β-strands with the framework oxygens. Our results suggest that L-lysine conformation strongly depends on both pH and hydration state influencing amino acids physico-chemical properties and intermolecular bond energies.

1. Introduction

α-amino acids are an important class of organic compounds which play an important role in drug delivery systems, pharmaceutical exploration for new drugs, as well as in food technology, biomaterial devices, plastics industry, medical implants, biosensors, and diagnostic assays [1,2]. However, amino acids applications often require strict purity standards, consequently, separation and purification of these biomolecules is a crucial task in production processes [3,4]. Amino acids separation and enrichment has been achieved by using different adsorbent materials such as organic resins [5], silica particles [6], carbon nanotubes [7] and magnetic silica nanoparticles [8]. In the last years, adsorption from aqueous solutions into zeolites [4,9–11] and mesoporous materials [12] has become increasingly widespread in separation and purification processes [13]. Lysine (Lys) is essential to animals since it affects their growth and health, and it is used in feed with a demand of 2.4 million metric tons in 2015 [14]. Lysine is commercially obtained via microbial-fermentation and purification is one of the critical steps of its production. Recently, it has been reported that zeolites can be successfully employed to recover amino acids from fermentation broth [15]. Very recently, Beltrami et al. [16] reported that L-Lys adsorbed in L zeolite assumes an α-helical conformation stabilized by the occurrence of strong H-bonds among the tail amino groups of lysine, co-adsorbed water molecules, and framework oxygens atoms. As far as concerns achiral MFI zeolites, Chen et al. [17] proved that achiral MFI zeolites show differential adsorption properties towards L- and D-Lys enantiomers in acid solution (pH < 2), thus potentially expanding the application of achiral zeolite even in chiral separations. In their work, Chen

* Corresponding author.
** Corresponding author.
E-mail addresses: annalisa.martucci@unife.it (A. Martucci), luisa.pasti@unife.it (L. Pasti).
[1] Present affiliation: ENEA, Italian National Agency for New Technologies, Energy and Sustainable Economic Development, Trisaia Research Centre, Rotondella, I-75,026, Italy.

https://doi.org/10.1016/j.micromeso.2021.111183
Received 5 March 2021; Received in revised form 11 May 2021; Accepted 13 May 2021
Available online 20 May 2021

Table 1
Properties and structure of L-Lys amino acid.

L-Lys	
Chemical formula	$C_6H_{14}N_2O_2$
Molar mass	146.19 g mol^{-1}
pK_a	2.2; 9.1; 10.7

Table 2
Details of data collection and structure refinements agreement indices.

	ZSM-$5_{(15)}$	ZSM-$5_{(37)}$	L-Lys-ZSM-$5_{(15)}$	L-Lys-ZSM-$5_{(37)}$
Wavelength (Å)	0.82700(1)			
Energy (keV)	15			
Refined 2θ (°) range	3–36			
N_{data}	8399	6399	6522	6522
N_{var}	153	233	239	239
R_{wp}	0.1130	0.1190	0.1280	0.1280
R_p	0.0901	0.0955	0.1058	0.1058
R_F^2	0.0817	0.0864	0.0925	0.0939

$R_p = \sum[Y_{io} - Y_{ic}]/\sum Y_{io}$; $R_{wp} = [\sum wi(Y_{io}-Y_{ic})^2/\sum wiY_{io}^2]^{0.5}$; $R_F^2 = \sum|F_o^2-F_c^2|/|F_o^2|$.

et al. [17] investigated the adsorption properties of MFI zeolite in acid (pH < 2.2) solution. However, depending on the degree of protonation of the amino and carboxyl groups, the net charge of an amino acid molecule changes greatly from positive or neutral to negative in an aqueous solution. Therefore, amino acids can show very different adsorption behaviors at different pH, since this parameter can strongly influence electrostatic attraction, covalent bonding, hydrogen bonding, and hydrophobic interactions with the adsorbent material. Indeed, the amino acids adsorption on microporous molecular sieves can be driven by various types of interaction, depending on the adsorbent features, the adsorption conditions and amino acids shape and size. In addition the physicochemical properties of ZSM-5 crystals, such as size, morphology, aluminum distribution strongly depend on the synthesis conditions and in particular on the choice of inorganic and/or organic structure-directing agents [18,19]. Furthermore, amino acid derivatives such as peptoids have been recently employed as zeolite growth modifiers. The chemical stability of peptoids, their facile and efficient synthesis offer the possibility to select tailored grown modifier to obtained designed zeolites physicochemical crystal properties [20]. The high number of factors affecting the amino acids adsorption make this process

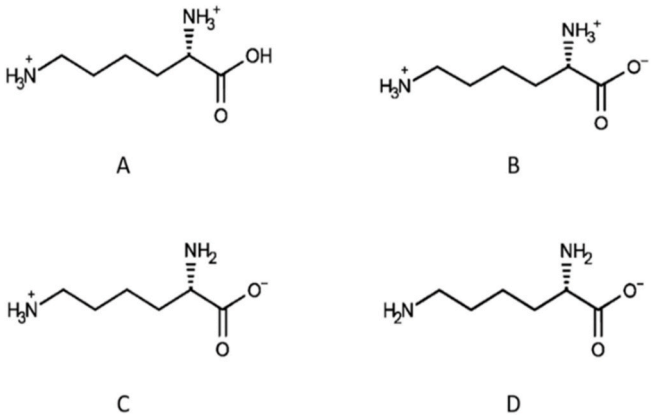

Fig. 2. Structures of L-Lys for different charge states.

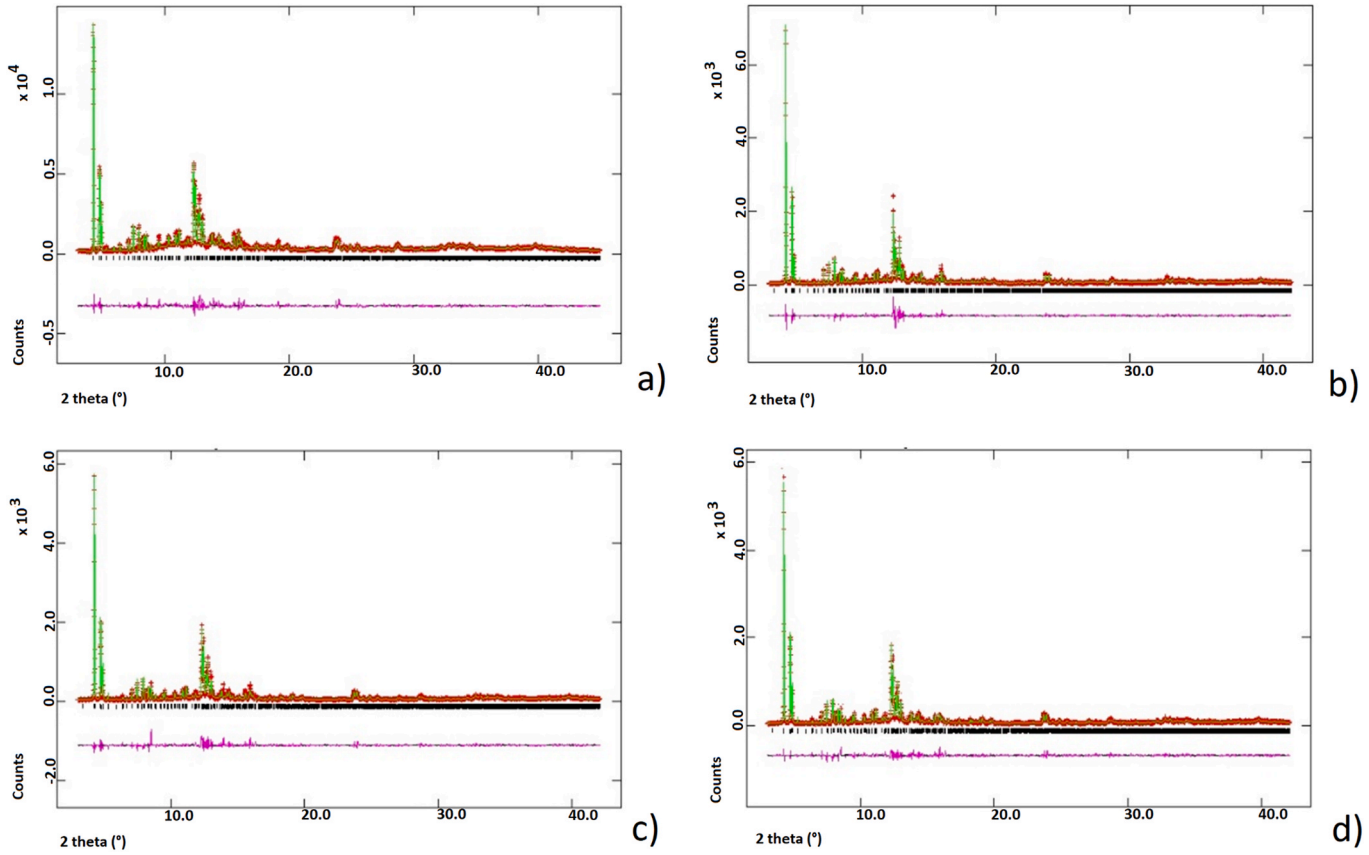

Fig. 1. Final Rietveld fit of synchrotron X-ray powder diffraction patterns for ZSM-5 zeolites (a) ZSM-$5_{(15)}$, (b) ZSM-$5_{(37)}$, (c) L-Lys-ZSM-$5_{(15)}$ and (d) L-Lys-ZSM-$5_{(37)}$. The experimentally observed data are indicated by crosses, the calculated pattern is the continuous line among crosses, and the lower curve is the weighted difference between calculated and observed patterns.

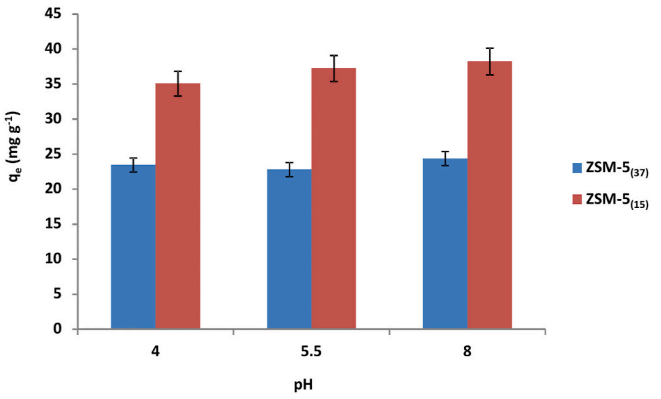

Fig. 3. Adsorbed quantity of L-Lys on ZSM-5$_{(15)}$ and ZSM-5$_{(37)}$ zeolites at different pH (initial L-Lys concentration 50 mg L^{-1}).

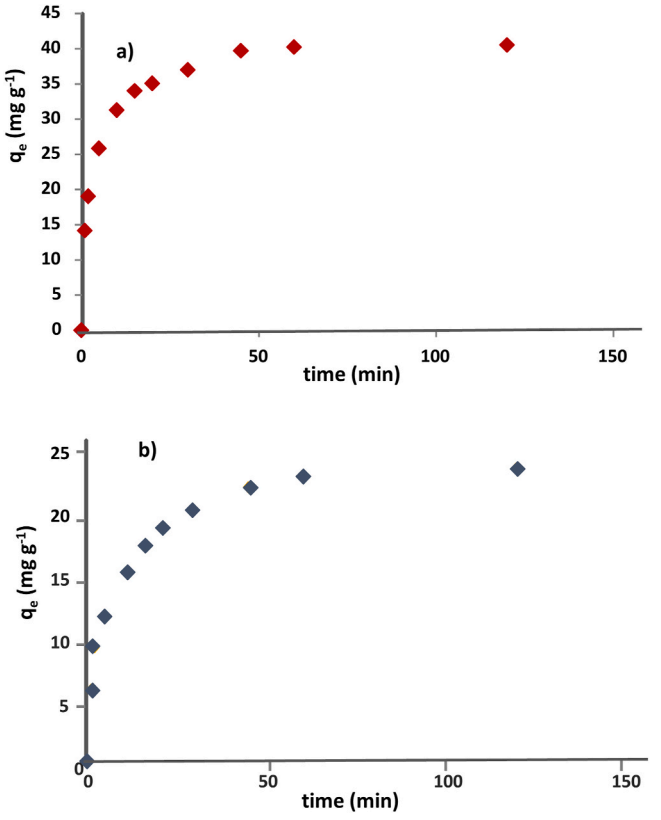

Fig. 4. Uptake of L-Lys on a) ZSM-5$_{(15)}$ and b) ZSM-5$_{(37)}$ *vs.* time (initial L-Lys concentration 80 mg L^{-1}).

Table 3
Parameters obtained by non-linear fitting of the uptake data using PFO and PSO models. The error is given as confidence interval at 95% of probability.

	k_1 (min^{-1})	q_e (mg L^{-1})	R^2	k_2 (g mg^{-1} min^{-1})	q_e (mg L^{-1})	R^2
ZSM-5$_{(15)}$	0.3 ± 0.11	37 ± 3	0.9464	0.010 ± 0.003	41 ± 2.1	0.9905
ZSM-5$_{(37)}$	0.2 ± 0.12	20.0 ± 0.4	0.9264	0.0072 ± 0.00052	23 ± 2.3	0.9887

particularly complex and a complete elucidation still deserves further investigations [21–23]. The goal of the present study is to evaluate the adsorption properties of two ZSM-5 zeolites (MFI topology), having silicon to aluminum ratio (Si/Al) equal to 15 and 37, respectively, towards L-Lys amino acid, chosen as an ideal benchmark structure because of its single sidechain amine group. ZSM-5 was selected as adsorbent because of its high surface area and 3D pore structure containing two intersecting 1D channels, both delimited by 10-membered rings (5.4 × 5.6 Å and 5.1 × 5.5 Å window sizes, respectively). With the purpose of gaining insight on the capability of ZSM-5 zeolite to adsorb L-Lys at intermediate pH, in this work we evaluate the kinetics and thermodynamics of the adsorption process in term of kinetic and equilibrium constants. ZSM-5 adsorbents were also characterized for their saturation capacity. In addition, structure refinements of high resolution X-ray diffraction data from synchrotron source allowed the investigation of the interactions between the adsorbate and the zeolite framework. This technique allowed to estimate bond lengths, indicating the presence of strong host-guest and guest-guest interactions of L-Lys inside the zeolitic framework.

2. Materials and methods

2.1. Zeolites

Two samples of H^+ form ZSM-5 zeolite were synthesized by hydrothermal synthesis technique [24] with Si/Al ratios equal to 37 and 15, and labelled as ZSM-5$_{(37)}$ and ZSM-5$_{(15)}$, respectively.

2.2. Amino acid

L-Lysine amino acid ((2S)-2,6-Diaminohexanoic acid) was provided by Sigma-Aldrich (Steinheim, Germany), with a purity of 99.8%. L-Lys structure and chemical properties are shown in Table 1.

2.3. Adsorption experiments

Equilibrium adsorption tests were performed by suspending ZSM-5 zeolites in aqueous solutions of L-Lys at different initial concentrations (5, 10, 20, 50, 70, 100, 150 and 200 mg L^{-1}) with a solid/liquid ratio of 1:1 (mg mL^{-1}). The suspensions were kept at 298 K under stirring for 18h at pH 5.5. The contact time was longer than the equilibration time determined by kinetics experiments.

To determine the adsorption kinetics, the L-Lys uptake was measured starting from a solution at concentration of 80 mg L^{-1}, after contact time equal to 1, 2, 5, 10, 20, 30, 45, 60, 120 min, with a zeolite/solution ratio of 1:1 (mg mL^{-1}), the suspensions were kept at 298 K under stirring. All experiments were carried out in duplicate.

An Agilent Technologies Capillary Electrophoresis (CE) series 7100 system (Santa Clara, CA, USA) was employed to quantify L-Lys in the solution before and after the contact with zeolites. The CE system was equipped with a diode array detector (DAD). For separations, extended light path (bubble cell) bare fused-silica capillaries (red G1600-61232 I. D.: 50 μm, total length: 64.5 cm, effective length: 56 cm, bubble factor: 3) obtained from Agilent Technologies (Santa Clara, CA, USA) were employed.

Hydrodynamic injection of the solutions was performed at a pressure of 10 mbar applied for 30 s. The detection wavelength of the CE-DAD system was 200 nm. Positive polarity (15 kV) was applied at the capillary inlet for the duration of the separation. The running buffer was a 50 mM solution of Na_2HPO_4 in MilliQ water, at pH 5.5 adjusted by adding H_3PO_4. The pH of the electrolyte was measured using an AMEL pHmeter (Milano, Italy). Before use, the capillary was pretreated through sequential flushing with 1 M NaOH for 5 min, 0.1 M NaOH for 5 min, MilliQ (Millipore, Bedford, MA, USA) grade water for 15 min and running buffer for 15 min. The capillary was also rinsed with water for 3 min, 0.1 M NaOH for 2 min, water for 3 min, and running buffer for 5 min between each run.

The amount of L-Lys adsorbed at equilibrium, q_e (mg g^{-1}), was calculated from the mass balance equation, Eq. (1):

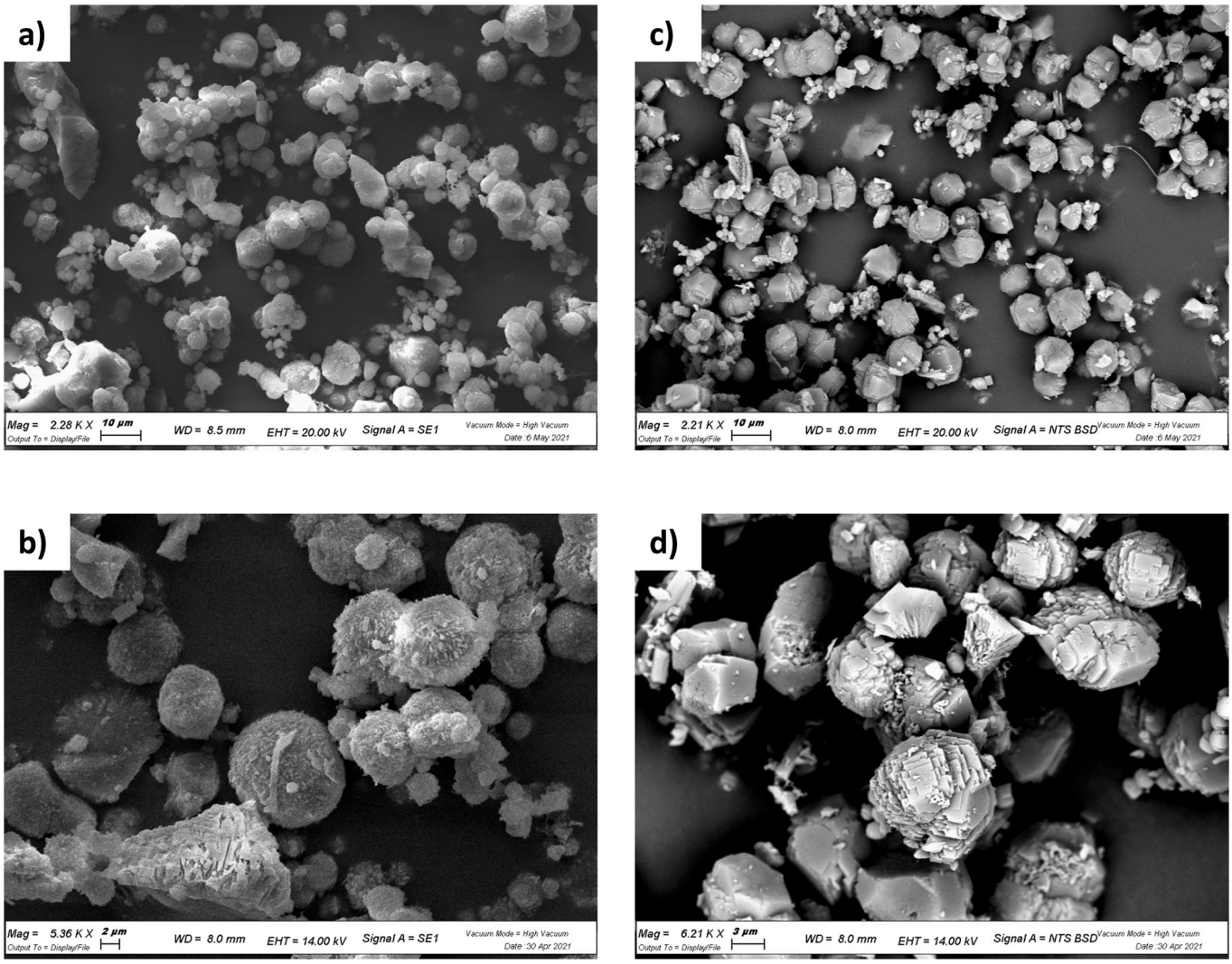

Fig. 5. SEM images: a) and b) ZSM-$5_{(15)}$, c) and d) ZSM-$5_{(37)}$.

$$q_e = \frac{(C_i - C_e)V}{m} \quad (1)$$

where C_i and C_e (mg L^{-1}) are the liquid-phase concentrations of L-Lys in the reference solution and at equilibrium, respectively; V (L) is the volume of the solution and m (g) is the mass of dry zeolite used. Samples of zeolites saturated with L-Lys were used for structural investigations. ZSM-$5_{(37)}$ and ZSM-$5_{(15)}$ (0.5 g) were suspended by continuous stirring in 500 mL of an 80 mg L^{-1} L-Lys aqueous solution at pH 5.5 at 298 K for 24 h. The zeolite was recovered by filtration, washed with 200 mL of MilliQ water and dried in oven at 300 K overnight before X-ray measurement.

2.4. Scanning Electron Microscopy

Scanning Electron Microscopy (SEM) imaging was obtained with a Zeiss Evo 40 electron microscope.

2.5. Synchrotron X-ray powder diffraction

Room temperature synchrotron data were collected at the MCX beamline of the Elettra Synchrotron Light Source (Trieste, Italy) [25,26] on a 4-circle Huber diffractometer equipped with a high-count rate fast scintillator detector preceded by a pair of slits with vertical aperture of 200 and 300 µm. ZSM-$5_{(37)}$ and ZSM-$5_{(15)}$ samples were loaded into an axially spinning borosilicate capillary (Ø = 0.5 mm). Details of powder patterns data collection are reported in Table 2.

2.6. Thermal analysis

Thermogravimetric (TG) and differential Thermal Analysis (DTA) curves were obtained through The Netzsch STA 409 PC LUXX® (Gerätebau, Germany) simultaneous TG/DTA thermogravimetric balance after L-Lys adsorption on both ZSM-$5_{(37)}$ and ZSM-$5_{(15)}$ samples. Thermal analyses were performed from 20 °C to 900 °C, with a heating rate of 10 °C min^{-1} under air flow (flow rate 20 mL min^{-1}).

2.7. Refinement strategy

Full profile Rietveld refinements were performed by means of the GSAS-EXPGUI software package [27,28] starting from the framework atomic coordinates of Van Koningsveld et al. [29]. Peaks profile was modelled through a Pseudo-Voigt function with the peak cut-off set to 0.01% of the peak intensity maximum, by means of two Gaussian terms (θ-independent *GW*, tan-θ dependent *GV*, respectively), and one Lorentzian broadening coefficient (tanθ-dependent *LY*) plus an asymmetry contribution (*asym*) and a term to reproduce the anisotropic contribution of the Lorentzian broadening (*stec*). Besides 18 shifted Chebyshev polynomial coefficients to fit the background and a shift contribution (*shift*) to account for the sample displacement, the refinements included

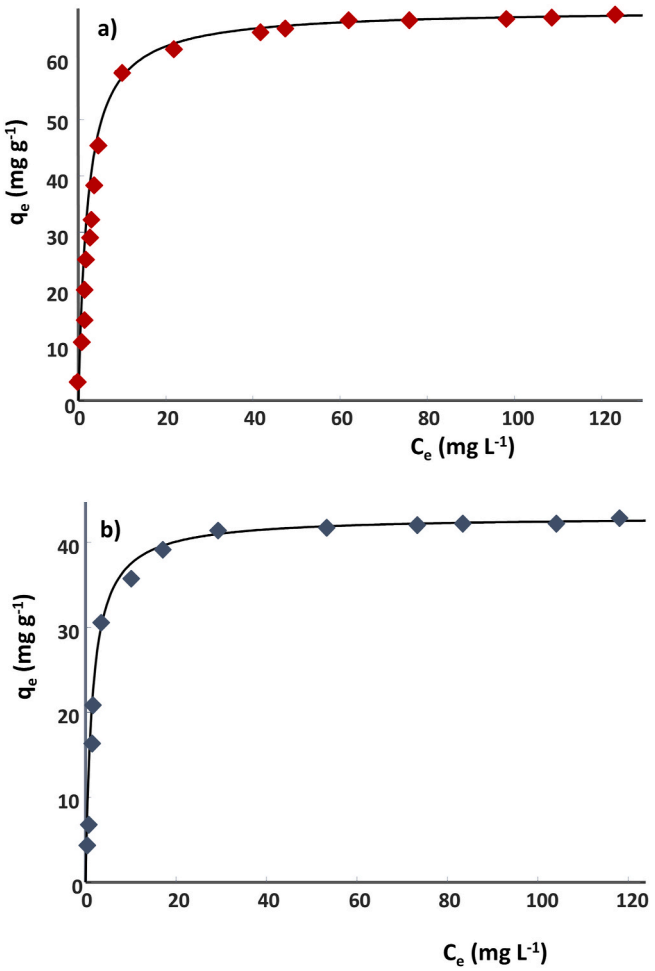

Fig. 6. Adsorption isotherms of L-Lys on: a) ZSM-5$_{(15)}$ and b) ZSM-5$_{(37)}$ at 298 K.

Table 4
Saturation capacities (q_S) and binding constants (b) for the adsorption of L-Lys. The error is given as confidence interval at 95% of probability.

	q_S (mg g^{-1})	b (L mg^{-1})	R^2
ZSM-5$_{(15)}$	65 ± 2.7	0.6 ± 0.23	0.9633
ZSM-5$_{(37)}$	44 ± 1.2	0.4 ± 0.14	0.9827

unit-cell parameters, atomic coordinates, and Atomic Displacement Parameters (ADPs, Uiso). During the refinement of the framework atomic coordinates, a set of soft constraints was applied to tetrahedral T–O and O–O bond distances (T–O = 1.60 Å and O–O = 2.60 Å, σ = 0.04). The restraint weight (F) was progressively lowered in the last refinement cycles until atomic coordinates were allowed to vary almost freely (*i.e.*, the calculated standard deviation of the bond lengths was smaller than the tolerance applied to the constrained bond distances). The Atomic Displacement Parameters (ADPs) were constrained in order to have the same value for the same atomic species. The atomic coordinates of extraframework molecules were derived from residuals of electron density calculated by mean of the Difference Fourier maps. In order to retain the L-Lys geometry, extraframework atomic coordinates were refined imposing soft constraints on C–C and N–C (*i.e.*, 1.40 Å, σ = 0.04 Å), and C–O (*i.e.*, 1.35 Å, σ = 0.04 Å) bond distances. The geometry of the L-Lys molecule was then optimized through a tool within the EXPO2014 software [30]. The so obtained framework and optimized extraframework set of atomic coordinates were then refined together by the GSAS program until the best agreement between experimental data and calculated pattern was reached. ADPs were constrained in order to have the same value for the same atomic species. The final fit of both Rietveld refinements is given in Fig. 1.

Details about data collection and structure refinements agreement indices are reported in Table 2. Framework atomic coordinates, site atomic fractions, and ADPs for both ZSM-5$_{(37)}$ and ZSM-5$_{(15)}$ before and after L-Lys adsorption are available as supplemental material in SI (Tables SI1–SI7). Extraframework atomic coordinates, atomic fraction and ADPs are listed in Table SI6. *T*–O bond distances and *T*–O–*T* bond angles are reported in Tables SI4 and SI7. Cif files are available as supplemental material in SI (Tables SI8-SI11).

3. Results and discussion

3.1. Effect of pH on sorption capacity

The effect of pH on the adsorption of L-Lys onto ZSM-5 was investigated in the 4–8 pH range. Properties of amino acids are modulated by the pH of aqueous solutions, acting on the type of functional group charged, hence driving structural modifications. The Lewis structure of L-Lys molecule for different charge states is shown in Fig. 2, determined on the basis of published dissociation constants (pKa): α-carboxyl group (2.2), α-amino group (9.1), and side-chain-amino group (10.7) [31]. At pH < 2.2 L-Lys is in the dicationic form: both amino groups are protonated, and the carboxyl group is undissociated (Fig. 2A). The cationic form prevails in the pH range 2.2–9.5 (Fig. 2B). Near the isoelectric point, close to pH 9.5, only the amino group of the side chain is protonated, and the α-amino group is not (Fig. 2C). Above pH 10.5 both amino groups are deprotonated (Fig. 2D). The pH range 4–8 was selected to avoid partial dissolution or degradation of zeolite in acidic and basic aqueous media. In such pH interval, adsorption should not be influenced by pH, since the prevailing form does not change [10]. However, the adsorption of lysine on ZSM-5 zeolite having a Si/Al equal to 30 has been reported to increase with the pH [4]. The data gathered from adsorption experiments at pH 4, 5.5 and 8 show that, within the experimental uncertainty, the L-Lys uptake is constant for a same zeolite composition, and it varies for different zeolite Si/Al ratio (see Fig. 3). Therefore, the interactions responsible for the adsorption between L-Lys and both the ZSM-5 tested are mainly driven by the ionic form of the amino acid more than from specific hydrophobic interactions. Since at pH 5.5 more than 99% of all lysine molecules adopt the cation two-site protonated form B [32], this pH value was selected for further investigations.

3.2. Kinetics experiments

To gain insight on the equilibrium time and the kinetics of the adsorption process, the L-Lys uptake (q_t) vs. time was measured. Fig. 4 shows that adsorption equilibrium is reached in about 60 min. The experimental data were modelled by using the pseudo first order (PFO) equation, given by Eq. (2):

$$q_t = q_e[1 - \exp(-k_1 t)] \quad (2)$$

where q_t, is the adsorbed quantity per unit mass after a contact time t and k_1 is the pseudo first-order kinetic constant.

In addition, a pseudo second order (PSO) relationship was employed to fit the data:

$$q_t = \frac{k_2 \; q_e^2 \; t}{1 + k_2 \; q_e \; t} \quad (3)$$

The kinetic parameters obtained by nonlinear fitting regression using Eqs. (2) and (3) are reported in Table 3.

It has been reported in the literature that the goodness of fitting is not a criterion sufficient to assess the mechanism underlying the adsorption process. However, the reliability of the fitted parameters could be employed to select the kinetic model [33,34]. From the comparison of

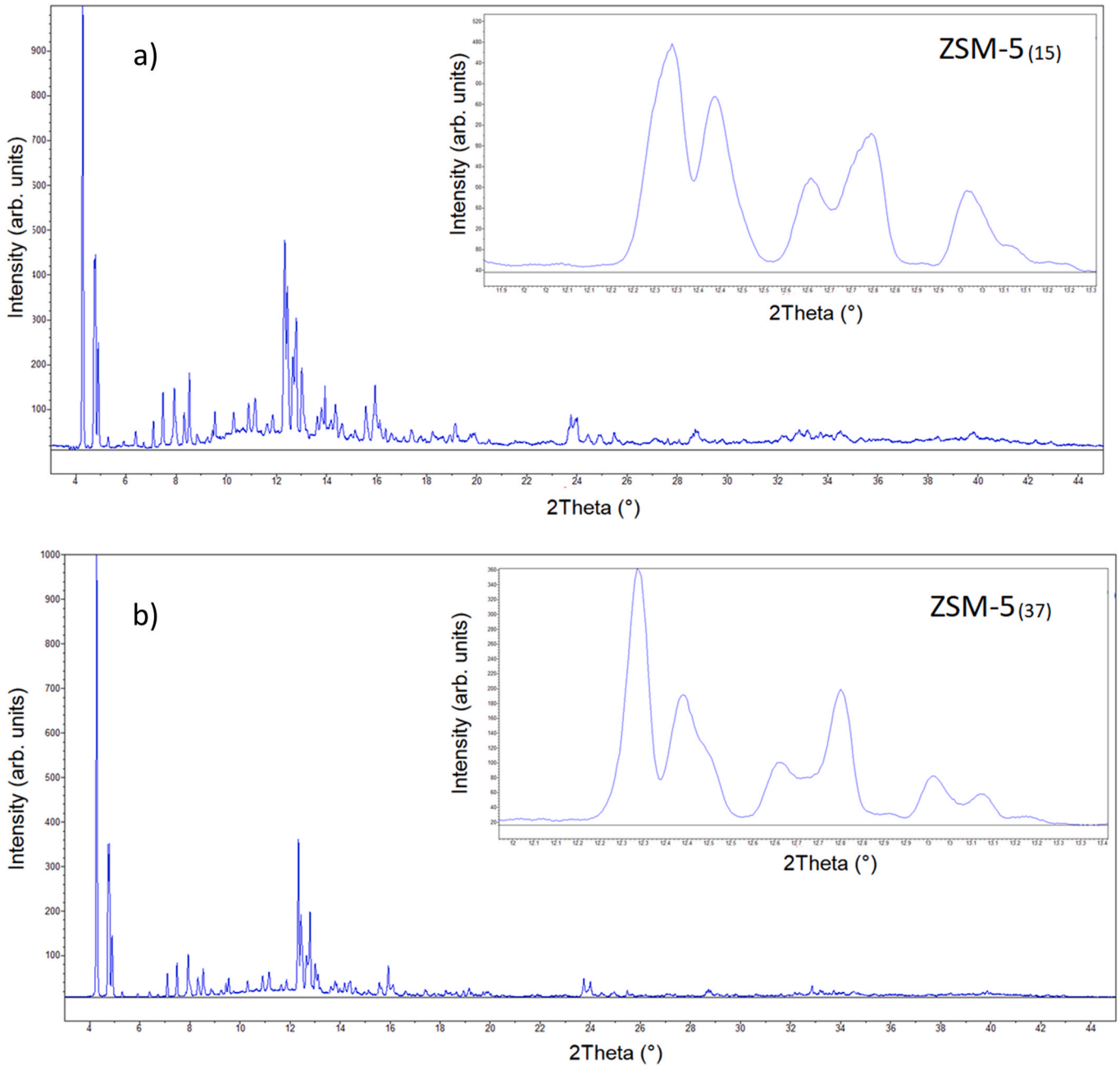

Fig. 7. Comparison between X-ray powder patterns of a) ZSM-$5_{(15)}$ and b) ZSM-$5_{(37)}$, respectively.

Table 5
Lattice parameters for ZSM-5 zeolites before and after L-Lys adsorption.

	ZSM-$5_{(15)}$	ZSM-$5_{(37)}$	L-Lys ZSM-$5_{(15)}$	L-Lys ZSM-$5_{(37)}$
Space Group	*Pnma*	$P2_1/n$	$P2_1/n$	$P2_1/n$
a (Å)	19.9485(9)	19.9113(6)	19.9111(5)	19.9075(5)
b (Å)	20.1511(10)	20.1367(5)	20.1324(5)	20.1316(4)
c (Å)	13.4200(8)	13.3961(5)	13.3944(4)	13.3905(3)
V (Å^3)	5394.6(5)	5370.9(3)	5369.0(2)	5366.3(2)
β (°)	90	90.492(3)	90.505(3)	90.517(2)

data in Table 3, it can be observed that the kinetic constants evaluated by PSO are more precise than those obtained by PFO. Scanning electron microscopy, reported in Fig. 5 showed a crystals size of about 8 μm, with the classical shape of MFI structure varying from prismatic to spherical shape [35]. Ruthven investigated the diffusion of amino acids such as glycine, alanine, and lysine in a hydrophilic KX-zeolite (1.1, 5.0, and 1.5 × 10–13 $m^2 s^{-1}$ at 5 °C) [36]. The diffusion coefficients values reported by Ruthven are comparable to those of sugars and other small organic molecules in zeolites having different structure and composition [37]. However, from these data it is difficult to estimate real diffusion path, and the contribution of diffusion to the adsorption kinetics since many factors such as framework deformations due to adsorption (see section 3.4), difference in the mobility of the molecule in the ZSM-5 channels, and specific host gest interactions come into play simultaneously. Consequently, to better estimate this parameter a computation approach, which lies beyond the scope of the present work, could be employed [38]. The adsorption process can indeed be governed by one or more steps such as film or external diffusion, pore diffusion, surface diffusion and adsorption on the pore surface, or a by a combination of more than one step through the adsorption process. It has been reported in Ref. [39] that the contribution of the intra-particle diffusion

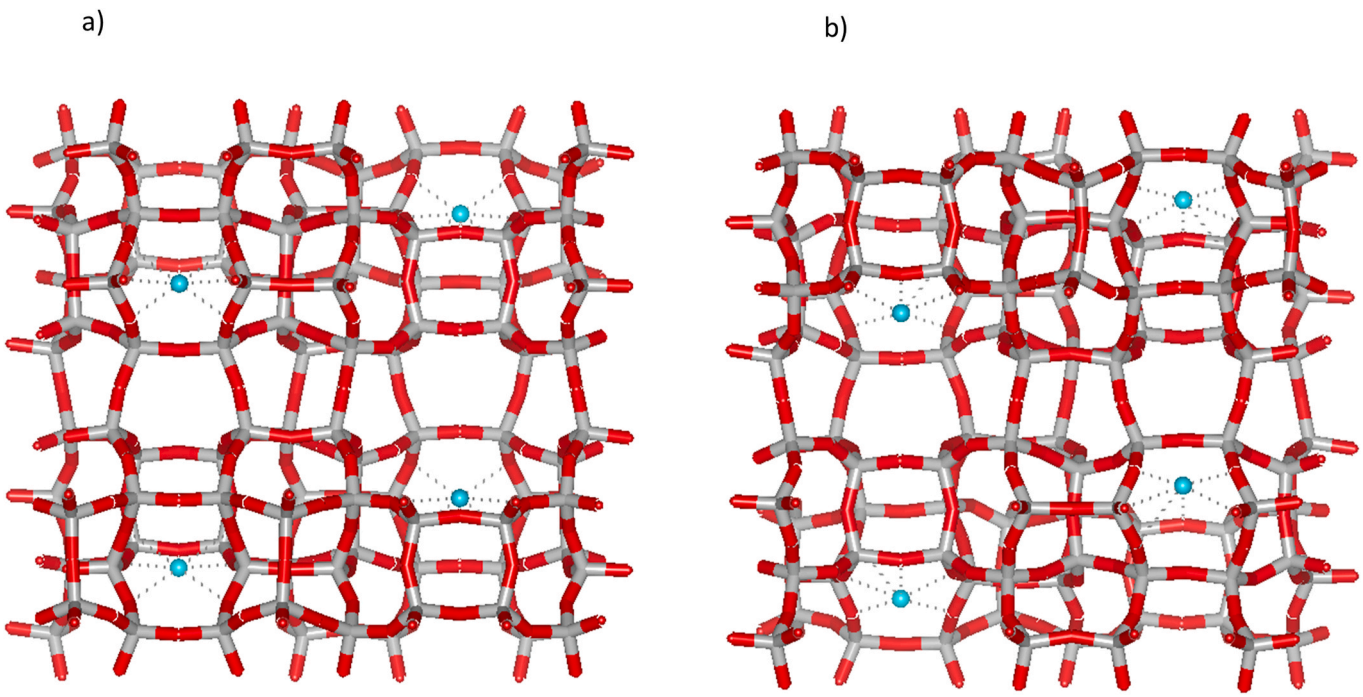

Fig. 8. Distribution of chemisorbed water molecules (light blue sphere) in a) ZSM-$5_{(15)}$ and b) ZSM-$5_{(37)}$ respectively, view along the [110] direction. (For interpretation of the references to colour in this figure legend, the reader is referred to the Web version of this article.)

resistance affecting adsorption process can be explored by using the Weber-Morris intraparticle diffusion model [40].

$$q_t = k_d\, t^{1/2} + C \tag{4}$$

where k_d is the intraparticle diffusion constant (mg g^{-1} $min^{-1/2}$) and C (mg g^{-1}) refers to a constant related to the thickness of the boundary layer. The data are reported in Figure SI1 in supplementary information, it can be seen that the data exhibit multi-linear plots, then two or more steps influence the sorption process [41].

3.3. Equilibrium adsorption results

The adsorption isotherms were obtained at 298K, by measuring the amount of adsorbed L-Lys from solution at different initial concentrations at constant temperature. The experimental data are reported in Fig. 6(a) and (b) for ZSM-$5_{(15)}$ and ZSM-$5_{(37)}$, respectively. For both zeolites, the data indicate that the shape of the isotherm curves is convex, showing a favorable adsorption for L-Lys. Data were fitted through a Langmuir model, Eq. (4):

$$q_e = \frac{q_s\ b\ C_e}{1 + \ b\ C_e} \tag{5}$$

where q_s is the saturation capacity of the zeolite and b is the binding constant. The applicability of Langmuir model to zeolitic systems has been proposed by Ruthven [42] and it has been already been employed to describe the adsorption of amino acids onto different zeolites including ZSM-5 [10,11,43–45].

In Table 4 the binding constants and saturation capacities for the adsorption of L-Lys on both ZSM-5 zeolites are reported. The parameters in Table 4 indicate that both saturation capacity and binding constant are larger for ZSM-$5_{(15)}$ than for ZSM-$5_{(37)}$. These differences are due to the different chemical composition of the two zeolites having different Si/Al ratio. This result can be explained based on a higher hydrophilicity of ZSM-$5_{(15)}$ which can positively affect the adsorption of the cationic form of L-Lys. In addition, the observed behavior agrees with those reported by Krohn and Tsapatsis [10].

3.4. Synchrotron X-ray powder diffraction results

The peak indexing of the ZSM-$5_{(15)}$ powder diffraction pattern evidences that the characteristic peak doublets of the monoclinic polymorph are not fully resolved (i.e. [311], [−313] and [313]), and only a peak broadening in the 8–14° 2θ range can be appreciated (Fig. 7a). Additionally, when the powder pattern was in the $P2_1/n$ space group the β angle of the monoclinic phase became very close to 90°, consequently Rietveld refinements of ZSM-$5_{(15)}$ sample was performed in the orthorhombic *Pnma* space group, with 12 independent tetrahedral T-sites and 26 framework oxygen atoms per unit-cell. On the contrary, powder diffraction pattern of ZSM-$5_{(37)}$ revealed a monoclinic symmetry (e.g., $P2_1/n$) with 24 independent T-sites and 48 framework oxygen atoms (Fig. 7b). The lattice parameters and unit-cell volume obtained through full profile Rietveld refinements of the investigated ZSM-5 samples are listed in Table 5.

ZSM-$5_{(37)}$ and ZSM-$5_{(15)}$ atomic coordinates, site atomic fraction, and and ADPs are reported in Table SI1 and SI2, respectively. Structural differences are exclusively dependent to their chemical composition (*i.e.*, to the different aluminum content) which plays a key role in the formation of zeolite framework defectivities and, consequently, in their structural features. Indeed, high content of aluminum within the zeolite framework causes internal stresses that mainly affect the orientation of the ZSM-5 twin domains. This reflects into the monoclinic β angle variation that becomes as wider as the higher the Si/Al ratio, thus determining a higher degree of "monoclinicity" [29,46,47]. Both ZSM-$5_{(15)}$ and ZSM-$5_{(37)}$, are characterized by a regular framework geometry, with mean tetrahedral bond distances ⟨T–O⟩ equal to 1.593 Å and mean intrapolyhedral bond angles ⟨O–T–O⟩ of 109.4°. Fourier maps calculated from the Rietveld refinements for both samples showed a definite build-up of electron density (site W in Tables SI1 and SI2) which was attributed to a low content of chemisorbed water molecules (corresponding to 1.5–2.5% in weight, on the basis of the refined occupancies) H-bonded to the framework oxygen atoms. Their distribution in both ZSM-$5_{(15)}$ and ZSM-$5_{(37)}$, is reported in Fig. 8a) and b) respectively.

The comparison of powder patterns collected before and after the L-Lys adsorption (Fig. 9), showed that although the separation between

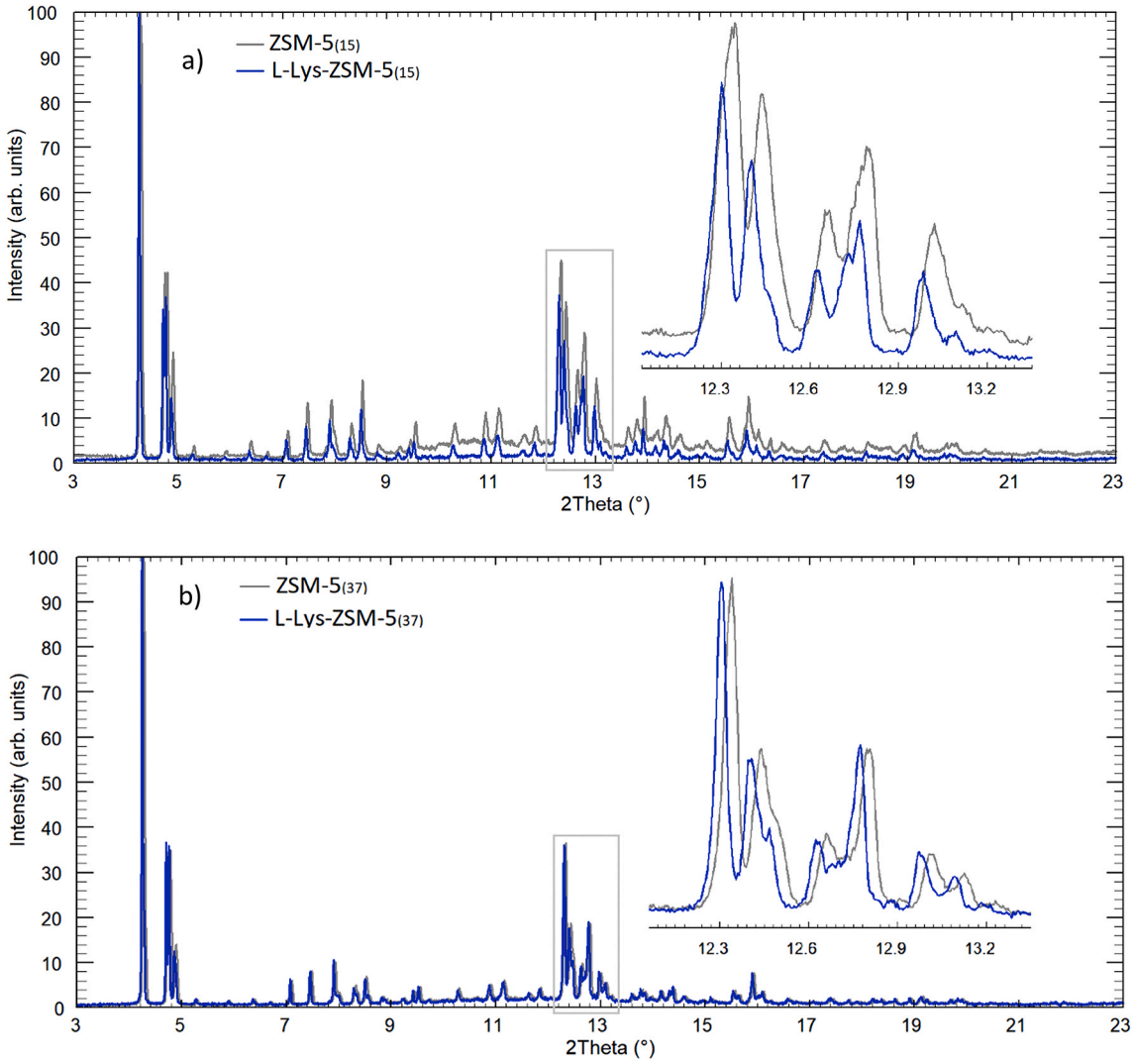

Fig. 9. Comparison between X-ray powder patterns before and after L-Lys adsorption: a) ZSM-$5_{(15)}$ and b) ZSM-$5_{(37)}$.

the angular positions of the [−313] and [313] reflections of the monoclinic phase is not well appreciated, the β angle refined is sufficiently wide to suggest the monoclinic symmetry of both systems (β = 90.505 (3)° and 90.517(2)° for ZSM-$5_{(15)}$ and ZSM-$5_{(37)}$, respectively). After the amino acid adsorption, refined lattice parameters highlighted only slight differences between the two loaded-samples (a = 19.9111(5) Å, b = 20.1324(5) Å, c = 13.3944(4) Å, V = 5369.02(25) Å^3 for ZSM-$5_{(15)}$; a = 19.9075(5) Å, b = 20.1316(4) Å, c = 13.3905(3) Å, V = 5366.29(22) Å^3, for ZSM-$5_{(37)}$), albeit the latter refined values are markedly shorter than those of unloaded samples (Table 5).

The analysis of residuals of electron density obtained from Difference Fourier maps revealed the presence of two adsorption sites attributed to the L-Lys adsorption within the ZSM-5 zeolite lattice. The first is located at the intersection of the sinusoidal and the straight channels (site A), whereas the second is within the sinusoidal channel (site B) in Fig. 10. The refinement of site occupancies showed that the two detected sites are partially occupied in loaded ZSM-5. On a whole, 4.8 and 6.7 wt% of L-Lys was detected within the ZSM-5(37) and the ZSM-5(15), respectively in good agreement with the data obtained from batch adsorption experiments (see Table 4). It has already been found that an increase in aluminum provides additional sites for the adsorption of cationic amino acids [10]. However, by considering, the adsorbed molecule per unit cell corresponding to ~1.9 and 2.8 molecules of L-Lys per unit cell and the corresponding Al/unit cell, which are 2.5 and 6.0 Al/UC) for ZSM-5(37) and the ZSM-5(15) respectively, it can be seen that the increase in the adsorption site is not proportional to the number of Al atom. Therefore, the adsorption sites in the investigated ZSM-5 are not equally accessible to the L-Lys molecules. However, to better clarify the role of Al concentration and distribution in ZSM-5 further research is needed, possibly comparing zeolites synthetized by using different structure-directing agents that can influence Al distribution [18]. Besides, an additional residual of electron density centered at x/a = 1/2, y/b = 1/2 and z/c = 0.0 fractional coordinates was detected and attributed to co-adsorbed water molecules (i.e., labelled as W1). As reported by Titus et al. [11] for NaZSM-5 the presence of an extremely low water content with respect to the amino acid content is due to the higher affinity of the zeolite towards the solute organic molecules. The location of extra-framework molecules in both ZSM-5(37) and ZSM-5(15) is similar, suggesting that the Si/Al ratio has a marginal effect over the adsorption sites of ZSM-5 (Fig. 10). On the basis of the refined site occupancies, 0.2 and 0.07 wt% of co-adsorbed water molecules were calculated for ZSM-5 (37) and ZSM-5(15), respectively. A simplified picture of the L-Lys configuration is shown in Fig. 11. L-Lys molecules at A site are arranged in a α-helical conformation with the α-carboxylic acid group (Oa1 and Oa2 sites, respectively) strongly interacting (e.g., H-bonds) with both W1 water molecule (Oa1-W1 = 2.34(2) Å) and framework oxygen atoms O20, O27 and O28 (Table 6).

The stabilization of this conformation is provided by the

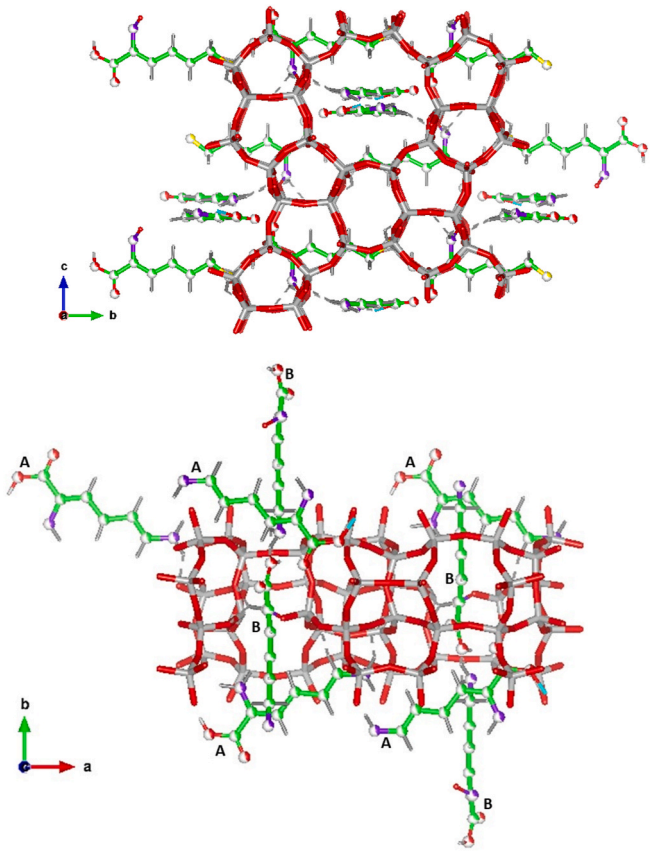

Fig. 10. Distribution of L-Lys in ZSM-5 view along the [100] and [001] direction, respectively. Green sphere: C atoms; light violet sphere: nitrogen ions; red sphere: oxygens atoms; stick: hydrogen atoms. (For interpretation of the references to colour in this figure legend, the reader is referred to the Web version of this article.)

simultaneous occurrence of strong H-bonds between the tail amino groups of L-Lys molecules (Na1) and the framework oxygens (Na1-O31 = 2.80(1) Å and Na1-O45 = 2.73(1) Å, respectively). In L-Lys molecules at B site, the carboxylic acid group is located close to the tail amino groups of the adjacent L-Lys molecules thus forming infinite hydrogen-bonding β-strands arranged as β-sheets (Table 6). The stabilization of L-Lys at B is emphasized by the simultaneous occurrence of H-bonds between the nitrogen (Nb2) of the side chain lysyl ($(CH_2)_4NH_2$) with the framework oxygen O18, O35 and O44, respectively (Table 6). No interactions with water molecules are highlighted. The presence of adsorption complexes involving hydrogen bond between carbonyl and the hydroxyl group of the amino acids were also found in NaZSM-5 [23]. In addition, in sodium exchanged ZSM-5, it has been reported that sodium cation in ZSM-5 can also interact with amino acids and stabilized the glycine zwitterion. The stereospecific bindings of L-Lys in MFI zeolites here reported differ strongly from those found recently by Chen et al. [17] at adsorption pH 1.0 and 2.2, respectively. The notable differences in both site occupancy factors and amino acid orientation suggest that L-Lys conformation strongly depends on both pH and hydration state. At pH lower than 2.5 Lys is mainly in its dicationic form (Fig. 2A) whereas at pH = 5.5 the cationic form (Fig. 2B) is prevalent. Discrepancies in the adsorption behavior of amino acids have been already reported, and in some cases, they can derive from differences in solution conditions such as pH. Indeed, pH strongly influence amino acids physico-chemical properties including intermolecular bond energies [32]. Therefore, direct microscopic investigations can help to better understand these phenomena. The α-helices at A site are stabilized by interactions with both framework oxygens and water molecules occupying the surrounding hydration shell. In the β-sheet conformation (B site), the absence of water-Lys interactions allows the formation of β-strands that fulfil the hydrogen-bonding potential associated with β-sheets. This model is in accordance with several investigations on structural flexibility of the lysine [48–50], summarizing, it can be proposed that the α-to-β transition of lysine has a non-hierarchical character due to the occurrence of structures. The lysine confinement is accompanied by changes in the atom framework deformations, that can be quantified by the analysis of the ellipticity parameter (*i.e.*, ε, defined as the ratio of the larger and the smaller O–O free diameter) of both sinusoidal and straight channels (SC channel: ε = 1.05 - ZZ channel entrance and exit: ε = 1.07 and 1.03 for ZSM-$5_{(37)}$; SC channel: ε = 1.05 - ZZ channel entrance and exit: 1.07 and 1.04 for ZSM-$5_{(15)}$, respectively, see Figure SI2). Figure SI2 (see Supplementary information) shows the dimensions of the zeolite channels systems as well as those of L-lysine obtained from the refined bond. Refined extraframework occupancies resulted in good agreement with thermal curves (Figure SI3 (a) and (b) in SI), that, between 100 and 900 °C, reveal a total weight loss of ~4.2 and 6.6 wt% for ZSM-$5_{(37)}$ and ZSM-$5_{(15)}$, respectively. The mass reduction observed in this thermal range is driven by the H_2O molecules desorption and the L-Lys decomposition (Figure SI3 a)). DTG peaks at 300 and 400 °C respectively (see Table 7 for temperature peak values) suggest that both L-Lys arrangement and allocation in zeolitic framework play a key role in its differential adsorption process. At the same time, these results clearly explain the different behavior reported by Chen. et al. [17]. These differences too, can be related to the different L-Lys forms with pH, as previously discussed. Within the same thermal range, the DTA curves of both investigated samples show the presence of two exothermic peaks in the range 300–600 °C reasonably ascribable to L-Lys oxidation or combustion processes since measurements were performed under air flow (Figure SI3 b)). The mass loss observed from room temperature to 100 °C, almost equal for both ZSM-$5_{(37)}$ and ZSM-$5_{(15)}$ samples (~2 wt%), is attributed to the release of surface adsorbed water, as suggested by the first intense endothermic peak of the DTA curve (Figure SI3 a)).

4. Conclusions

The multitechnical approach used to study the sorption capacity of ZSM-5 zeolites, with different Si/Al ratio, towards the L-Lys amino acid allowed to probe the efficiency of ZSM-5 in encapsulating this organic molecule. The kinetic and equilibrium constants of the adsorption processes estimated for both the zeolites show that zeolite composition play an important role in the adsorption in terms of sites occupancy, whilst no significant differences were found in adsorption sites location and interactions. Both the saturation capacity and the binding constant decrease as the hydrophilicity of the adsorbent material decreases. In addition, investigations at atomistic level performed with synchrotron radiation, indicate the adsorption of L-Lys in ZSM-5 in two different adsorption sites and with different conformation. L-Lys molecules at the intersection of the sinusoidal and the straight channels are arranged in a α-helical conformation stabilized by the simultaneous occurrence of strong H-bonds among the amino groups of L-Lys molecules, the framework oxygens, and the co-adsorbed water. L-Lys molecules within the sinusoidal channel are arranged as β-sheets forming infinite hydrogen-bonding β-strands with the framework oxygens. These results suggest that L-Lys conformation strongly depends on both pH and hydration state influencing amino acids physico-chemical properties and intermolecular bond energies. All data gained suggest that ZSM-5 is a performing sorbent material for the L-Lys compound and can be useful in capture amino acids from aqueous matrix.

CRediT authorship contribution statement

Tatiana Chenet: Writing – original draft, Methodology. **Annalisa Martucci:** Writing – review & editing, Conceptualization. **Mirco**

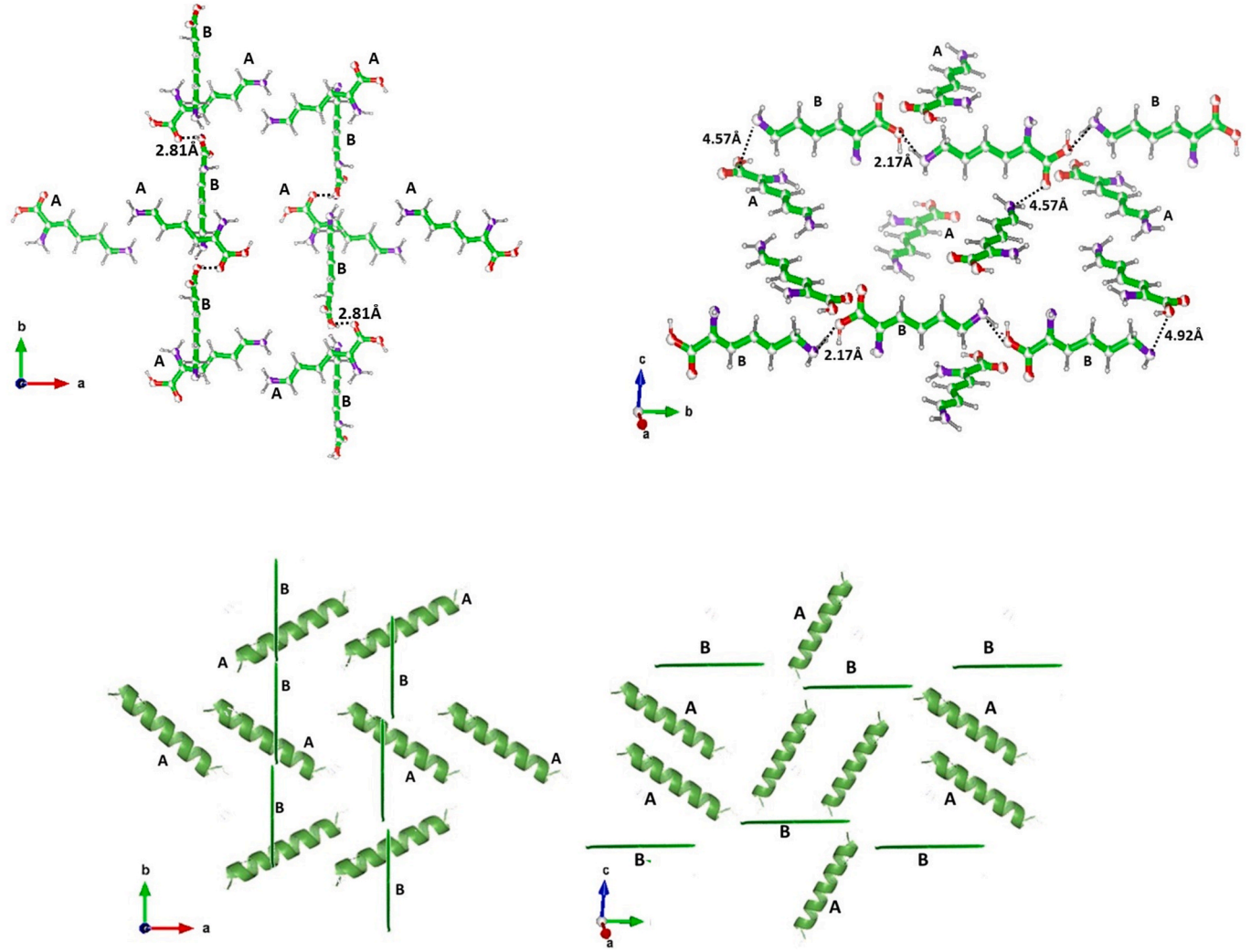

Fig. 11. Supramolecular assembly of L-Lys showing the α-helical (site A) and β-sheets (site B) configurations.

Table 6
Bond distances between extraframework molecules and framework oxygen atoms.

Bond Length (Å)	ZSM-5$_{(37)}$	ZSM-5$_{(15)}$
C98a-O20	2.90(3)	2.92(1)
C98a-O28	3.18(2)	3.14(1)
C99a-O31	2.74(4)	2.70(1)
C99a-O44	2.88(4)	2.91(2)
C101b-O18	2.86(1)	2.93(2)
C101b-O25	2.93(2)	2.97(3)
Na1-O31	2.80(1)	2.76(1)
Na1-O45	2.73(1)	2.68(2)
Oa1-O27	2.85(5)	2.87(3)
Oa1-O28	2.48(2)	2.48(1)
Oa1-W1	2.34(2)	2.36(3)
Oa2-O20	2.33(1)	2.32(1)
Oa2-O28	2.88(3)	2.83(2)
Oa2-Ob1	2.96(2)	2.98(1)
Oa2-Ob2	2.14(2)	2.12(1)
Nb1-O15	2.98(2)	2.96(3)
Nb1-O41	2.44(1)	2.47(1)
Ob1-O26	2.75(2)	2.87(3)
Nb2-O18	2.24(1)	2.27(3)
Nb2-O35	2.78(5)	2.74(4)
Nb2–O44	2.88(2)	2.85(3)

Table 7
DTG peaks observed in ZSM-5$_{(15)}$ and ZSM-5$_{(37)}$ after L-Lys adsorption. The data are compared with those reported by Chen et al. [17] (*).

	Peak 1 (°C)	Peak 2 (°C)	Peak 3 (°C)	Peak 4 (°C)
ZSM-5$_{(15)}$	87.3	299.1	405.0	611.7
ZSM-5$_{(37)}$	87.3	299.1	399.9	546.2
ZSM-5 L-1.0*	161.0	235.7	272.5	465.0
ZSM-5 D-1.0*	150.0	232.2	273.2	467.8
ZSM-5 L-2.2*	168.3	235.0	265.8	445.7
ZSM-5 D-2.2*	157.0	233.2	268.7	460.3

Cescon: Investigation. **Giulia Vergine:** Investigation. **Giada Beltrami:** Investigation. **Lara Gigli:** Methodology. **Matteo Ardit:** Data curation. **Massimo Migliori:** Writing – review & editing. **Enrico Catizzone:** Investigation. **Girolamo Giordano:** Formal analysis. **Luisa Pasti:** Conceptualization, Supervision.

Declaration of competing interest

The authors declare that they have no known competing financial interests or personal relationships that could have appeared to influence the work reported in this paper.

Acknowledgements

The research leading to these results has received funding from the Ministry of Education, University and Research (MIUR) under the PRIN 2017 program grant agreement n° 2017Y2PAB8_003 and from MIUR Department of Excellence funds, DM n.262, Budget Law 2017.

Appendix A. Supplementary data

Supplementary data to this article can be found online at https://doi.org/10.1016/j.micromeso.2021.111183.

References

[1] W. Notz, F. Tanaka, C.F. Barbas, Enamine-based organocatalysis with proline and diamines: the development of direct catalytic asymmetric aldol, mannich, michael, and Diels−Alder reactions, Acc. Chem. Res. 37 (2004) 580–591, https://doi.org/10.1021/ar0300468.
[2] S.L. Bourke, J. Kohn, Polymers derived from the amino acid l-tyrosine: polycarbonates, polyarylates and copolymers with poly(ethylene glycol), Adv. Drug Deliv. Rev. 55 (2003) 447–466, https://doi.org/10.1016/S0169-409X(03)00038-3.
[3] M. Meng, L. Stievano, J.-F. Lambert, Adsorption and thermal condensation mechanisms of amino acids on oxide supports. 1. Glycine on silica, Langmuir 20 (2004) 914–923, https://doi.org/10.1021/la035336b.
[4] S. Munsch, M. Hartmann, S. Ernst, Adsorption and separation of amino acids from aqueous solutions on zeolites, Chem. Commun. (2001) 1978–1979, https://doi.org/10.1039/b105333g.
[5] H. Anasthas, V. Gaikar, Adsorption of acetic acid on ion-exchange resins in non-aqueous conditions, React. Funct. Polym. 47 (2001) 23–35, https://doi.org/10.1016/S1381-5148(00)00066-3.
[6] M.D. Saikia, Studies on adsorption of amino acids on β-cyclodextrin bonded to silica particles, Colloids Surfaces A Physicochem. Eng. Asp 329 (2008) 177–183, https://doi.org/10.1016/j.colsurfa.2008.07.007.
[7] M.D. Ganji, Density functional theory based treatment of amino acids adsorption on single-walled carbon nanotubes, Diam. Relat. Mater. 18 (2009) 662–668, https://doi.org/10.1016/j.diamond.2008.11.021.
[8] S. Cheng, H. Yan, C. Zhao, The synergistic effect between hydrophobic and electrostatic interactions in the uptake of amino acids by strongly acidic cation-exchange resins, J. Chromatogr. A 1108 (2006) 43–49, https://doi.org/10.1016/j.chroma.2005.12.101.
[9] R. Wijntje, H. Bosch, A.B. de Haan, P.J.T. Bussmann, Influencing the selectivity of zeolite Y for triglycine adsorption, J. Chromatogr. A 1142 (2007) 39–47, https://doi.org/10.1016/j.chroma.2006.10.056.
[10] J.E. Krohn, M. Tsapatsis, Amino acid adsorption on zeolite β, Langmuir 21 (2005) 8743–8750, https://doi.org/10.1021/la0511788.
[11] E. Titus, A.K. Kalkar, V.G. Gaikar, Equilibrium studies of adsorption of amino acids on NaZSM-5 zeolite, Colloids Surfaces A Physicochem. Eng. Asp 223 (2003) 55–61, https://doi.org/10.1016/S0927-7757(03)00131-6.
[12] Q. Gao, W. Xu, Y. Xu, D. Wu, Y. Sun, F. Deng, W. Shen, Amino acid adsorption on mesoporous materials: influence of types of amino acids, modification of mesoporous materials, and solution conditions, J. Phys. Chem. B 112 (2008) 2261–2267, https://doi.org/10.1021/jp0763580.
[13] S. Lacasta, V. Sebastián, C. Casado, A. Mayoral, P. Romero, A. Larrea, E. Vispe, P. López-Ram-de-Viu, S. Uriel, J. Coronas, Chiral imprinting with amino acids of ordered mesoporous silica exhibiting enantioselectivity after calcination, chem, Materials 23 (2011) 1280–1287, https://doi.org/10.1021/cm1032546.
[14] Z. Chen, G. Liu, J. Zhang, J. Bao, A preliminary study on l-lysine fermentation from lignocellulose feedstock and techno-economic evaluation, Bioresour, Technol. 271 (2019) 196–201, https://doi.org/10.1016/j.biortech.2018.09.098.
[15] A. Faisal, M. Holmlund, M. Ginesy, A. Holmgren, J. Enman, J. Hedlund, M. Grahn, Recovery of l -arginine from model solutions and fermentation broth using zeolite-Y adsorbent, ACS Sustain. Chem. Eng. 7 (2019) 8900–8907, https://doi.org/10.1021/acssuschemeng.9b00918.
[16] G. Beltrami, A. Martucci, L. Pasti, T. Chenet, M. Ardit, L. Gigli, M. Cescon, E. Suard, L−Lysine amino acid adsorption on zeolite L: a combined synchrotron, X-ray and neutron diffraction study, Chemistry 9 (2020) 978–982, https://doi.org/10.1002/open.202000183.
[17] T. Chen, B. Huang, S. Day, C.C. Tang, S.C.E. Tsang, K. Wong, T.W.B. Lo, Differential adsorption of <scp>l</scp> - and <scp>d</scp> -lysine on achiral MFI zeolites as determined by synchrotron X-ray powder diffraction and thermogravimetric analysis, Angew. Chem. 132 (2020) 1109–1113, https://doi.org/10.1002/ange.201909352.
[18] A. Chawla, R. Li, R. Jain, R.J. Clark, J.G. Sutjianto, J.C. Palmer, J.D. Rimer, Cooperative effects of inorganic and organic structure-directing agents in ZSM-5 crystallization, Mol. Syst. Des. Eng 3 (2018) 159–170, https://doi.org/10.1039/C7ME00097A.
[19] M.K. Choudhary, M. Kumar, J.D. Rimer, Regulating nonclassical pathways of silicalite-1 crystallization through controlled evolution of amorphous precursors, Angew. Chem. 131 (2019) 15859–15863, https://doi.org/10.1002/ange.201908751.
[20] R. Li, A. Smolyakova, G. Maayan, J.D. Rimer, Designed peptoids as tunable modifiers of zeolite crystallization, Chem. Mater. 29 (2017) 9536–9546, https://doi.org/10.1021/acs.chemmater.7b03798.
[21] Z. Chen, J. Zhang, B. Yu, G. Zheng, J. Zhao, M. Hong, Amino acid mediated mesopore formation in LTA zeolites, J. Mater. Chem. 4 (2016) 2305–2313, https://doi.org/10.1039/C5TA09860B.
[22] N. Kitadai, T. Yokoyama, S. Nakashima, ATR-IR spectroscopic study of L-lysine adsorption on amorphous silica, J. Colloid Interface Sci. 329 (2009) 31–37, https://doi.org/10.1016/j.jcis.2008.09.072.
[23] B. Boekfa, P. Pantu, J. Limtrakul, Interactions of amino acids with H-ZSM-5 zeolite: an embedded ONIOM study, J. Mol. Struct. 889 (2008) 81–88, https://doi.org/10.1016/j.molstruc.2008.01.026.
[24] F. Frusteri, G. Bonura, C. Cannilla, G. Drago Ferrante, A. Aloise, E. Catizzone, M. Migliori, G. Giordano, Stepwise tuning of metal-oxide and acid sites of CuZnZr-MFI hybrid catalysts for the direct DME synthesis by CO2 hydrogenation, Appl. Catal. B Environ. 176–177 (2015) 522–531, https://doi.org/10.1016/j.apcatb.2015.04.032.
[25] L. Rebuffi, J.R. Plaisier, M. Abdellatief, A. Lausi, P. Scardi, MCX: a synchrotron radiation beamline for X-ray diffraction line profile Analysis, Z. Anorg. Allg. Chem. 640 (2014) 3100–3106, https://doi.org/10.1002/zaac.201400163.
[26] J.R. Plaisier, L. Nodari, L. Gigli, E.P. Rebollo San Miguel, R. Bertoncello, A. Lausi, The X-ray diffraction beamline MCX at Elettra: a case study of non-destructive analysis on stained glass, ACTA IMEKO 6 (2017) 71, https://doi.org/10.21014/acta_imeko.v6i3.464.
[27] A.C. Larson, R.B. Von Dreele, L. Alamos, Laur, 1994, pp. 86–748.
[28] B.H. Toby, EXPGUI, a graphical user interface for GSAS, J. Appl. Crystallogr. 34 (2001) 210–213, https://doi.org/10.1107/S0021889801002242.
[29] H. van Koningsveld, Localization of non-framework species in MFI, J. Mol. Catal. Chem. 134 (1998) 89–95, https://doi.org/10.1016/S1381-1169(98)00025-9.
[30] A. Altomare, C. Cuocci, C. Giacovazzo, A. Moliterni, R. Rizzi, N. Corriero, A. Falcicchio, EXPO2013 : a kit of tools for phasing crystal structures from powder data, J. Appl. Crystallogr. 46 (2013) 1231–1235, https://doi.org/10.1107/S0021889813013113.
[31] N. Kitadai, T. Yokoyama, S. Nakashima, ATR-IR spectroscopic study of L-lysine adsorption on amorphous silica, J. Colloid Interface Sci. 329 (2009) 31–37, https://doi.org/10.1016/j.jcis.2008.09.072.
[32] D. Nolting, E.F. Aziz, N. Ottosson, M. Faubel, I.V. Hertel, B. Winter, pH-induced protonation of lysine in aqueous solution causes chemical shifts in X-ray photoelectron spectroscopy, J. Am. Chem. Soc. 129 (2007) 14068–14073, https://doi.org/10.1021/ja0729711.
[33] J.-P. Simonin, On the comparison of pseudo-first order and pseudo-second order rate laws in the modeling of adsorption kinetics, Chem. Eng. J. 300 (2016) 254–263, https://doi.org/10.1016/j.cej.2016.04.079.
[34] W. Plazinski, W. Rudzinski, A. Plazinska, Theoretical models of sorption kinetics including a surface reaction mechanism: a review, Adv, Colloid Interface Sci. 152 (2009) 2–13, https://doi.org/10.1016/j.cis.2009.07.009.
[35] T. Armaroli, L.J. Simon, M. Digne, T. Montanari, M. Bevilacqua, V. Valtchev, J. Patarin, G. Busca, Effects of crystal size and Si/Al ratio on the surface properties of H-ZSM-5 zeolites, Appl. Catal. Gen. 306 (2006) 78–84, https://doi.org/10.1016/j.apcata.2006.03.030.
[36] C.B. Ching, D.M. Ruthven, Sorption and diffusion of some amino acids in KX zeolite crystals, Chem. Eng. J. 40 (1989), https://doi.org/10.1016/0300-9467(89)80045-0.
[37] D.C. Gernat, R. Rozenbroek, E.R. Brouwer, L.A.M. van der Wielen, M. Ottens, Mass transfer limitations in binderless ZSM-5 zeolite granules during adsorption of flavour compounds from aqueous streams, J. Chem. Technol. Biotechnol. 95 (2020) 3134–3148, https://doi.org/10.1002/jctb.6491.
[38] I.B. Losada, P. Grobas-Illobre, A. Misturini, J. Polaina, Y. Seminovski, G. Sastre, Separation of an aqueous mixture of 6-kestose/sucrose with zeolites: a molecular dynamics simulation, Microporous Mesoporous Mater. 319 (2021), 111031, https://doi.org/10.1016/j.micromeso.2021.111031.
[39] H. Liu, L. Long, X. Weng, S. Zheng, Z. Xu, Efficient removal of tetrabromobisphenol A using microporous and mesoporous carbons: the role of pore structure,, Microporous Mesoporous Mater. 298 (2020), https://doi.org/10.1016/j.micromeso.2020.110052.
[40] F.C. Wu, R.L. Tseng, R.S. Juang, Initial behavior of intraparticle diffusion model used in the description of adsorption kinetics, Chem. Eng. J. 153 (2009) 1–8, https://doi.org/10.1016/j.cej.2009.04.042.
[41] T. Yao, L. Qiao, K. Du, High tough and highly porous graphene/carbon nanotubes hybrid beads enhanced by carbonized polyacrylonitrile for efficient dyes adsorption, Microporous Mesoporous Mater. 292 (2020), https://doi.org/10.1016/j.micromeso.2019.109716.
[42] D.M. Ruthven, A simple theoretical isotherm for zeolites: further comments, Zeolites 2 (1982) 242–243, https://doi.org/10.1016/S0144-2449(82)80062-6.
[43] J.E. Krohn, M. Tsapatsis, Phenylalanine and arginine adsorption in zeolites X, Y, and β, Langmuir 22 (2006) 9350–9356, https://doi.org/10.1021/la061743m.
[44] K. Stückenschneider, J. Merz, G. Schembecker, Molecular interaction of amino acids with acidic zeolite BEA: the effect of water, J. Phys. Chem. C 118 (2014) 5810–5819, https://doi.org/10.1021/jp411734j.
[45] A.I. Lupulescu, M. Kumar, J.D. Rimer, A facile strategy to design zeolite L crystals with tunable morphology and surface architecture,, J. Am. Chem. Soc. 135 (2013) 6608–6617, https://doi.org/10.1021/ja4015277.
[46] N. Kamiya, W. Iwama, T. Kudo, T. Nasuno, S. Fujiyama, K. Nishi, Y. Yokomori, Determining the structure of a benzene7.2-silicalite-1 zeolite using a single-crystal X-ray method, Acta Crystallogr. Sect. B Struct. Sci. 67 (2011) 508–515, https://doi.org/10.1107/S0108768111038560.

[47] H. van Koningsveld, F. Tuinstra, J.C. Jansen, H. van Bekkum, On the preparation of a monoclinic (nearly) single crystal of zeolite HZSM-5, Zeolites 9 (1989) 253–256, https://doi.org/10.1016/0144-2449(89)90035-3.
[48] Ł. Szyc, S. Pilorz, B. Czarnik-Matusewicz, FTIR-ATR investigations of an α-helix to β-sheet conformational transition in poly(l-lysine), J. Mol. Liq. 141 (2008) 155–159, https://doi.org/10.1016/j.molliq.2008.04.016.
[49] A.V. Mikhonin, N.S. Myshakina, S.V. Bykov, S.A. Asher, UV resonance Raman determination of polyproline II, extended 2.5 1 -helix, and β-sheet Ψ angle Energy landscape in poly- l -lysine and poly- l -glutamic acid, J. Am. Chem. Soc. 127 (2005) 7712–7720, https://doi.org/10.1021/ja044636s.
[50] R.D. JiJi, G. Balakrishnan, Y. Hu, T.G. Spiro, Intermediacy of poly(<scp>l</scp> -proline) II and β-strand conformations in poly(<scp>l</scp> -lysine) β-sheet formation probed by temperature-jump/UV resonance Raman spectroscopy †, Biochemistry 45 (2006) 34–41, https://doi.org/10.1021/bi051507v.